Available online at www.sciencedirect.com
SCIENCE DIRECT®
ELSEVIER Mathematical and Computer Modelling 39 (2004) 991–1003
MATHEMATICAL AND COMPUTER MODELLING
www.elsevier.com/locate/mcm

Thermal Analysis of the Grinding Process

R. J. GU
Department of Mechanical Engineering, Oakland University
Rochester, MI, U.S.A.

M. SHILLOR
Department of Mathematical Sciences, Oakland University
Rochester, MI, U.S.A.

G. C. BARBER
Department of Mechanical Engineering, Oakland University
Rochester, MI, U.S.A.

T. JEN
Department of Mechanical Engineering, University of Wisconsin
Milwaukee, WI, U.S.A.

(Received and accepted July 2003)

Abstract—A two-dimensional mathematical model for the thermal aspects of a grinding process is presented. The model includes heat conduction in the grinding wheel, workpiece, and coolant. The heat generation through friction, heat loss to the environment as well as debris, and the interaction among the three components are described in detail. A finite-element algorithm is implemented to solve the nonlinear problem. Numerical results, such as temperatures in the grinding wheel and workpiece, are presented. © 2004 Elsevier Ltd. All rights reserved.

Keywords—Coolant, Friction, Grinding, Heat transfer, FEA.

NOMENCLATURE

b	thickness of fluid; m	h, h_F, h_{GW}	heat transfer coefficients from grinding wheel or workpiece to ambient air, from fluid to grinding wheel or workpiece, and between the grinding wheel and workpiece
c_G, c_W, c_F	specific heat of grinding wheel, workpiece, and fluid, respectively; J/kg-K	i, j, l	indices
D_0	average grain size; m	K_G, K_W, K_F	thermal conductivity of grinding wheel, workpiece, and fluid, respectively; W/m-K
F_0	maximum contact pressure; MPa	n	number of grains in the grinding zone
F_a	total applied force on grinding wheel; N		
g	grinding rate		

The authors acknowledge the financial support from a NSF-GOLI grant.

0895-7177/04/$ - see front matter doi:10.1016/j.mcm2003.07.009

n_G, n_W	unit outward normal to grinding wheel, workpiece
p	contact pressure; MPa
P_i	power generated from the friction force; N.m/s
r_G	radius of grinding wheel; m
s	coordinate along the grinding zone; m
s_l	size of grinding zone; m
$t, \Delta t$	time, time step size; sec.
v, v_l	feed speed of the workpiece, and velocity component of a point; m/s
α	fraction of contact of grain to grinding zone
β	parameter chosen as 0.5
ϕ_j, φ_j	one- and two-dimensional weighting functions
η_k, ψ_k	one- and two-dimensional linear interpolation functions
λ	parameter chosen as 0.5
μ	coefficient of friction
$\theta_G, \theta_W, \theta_F$	temperatures in grinding wheel, workpiece, and fluid, respectively; °C
θ_∞	ambient temperature; °C
$\Theta_{Gk}, \Theta_{Wk}, \Theta_{Fk}$	nodal temperature of grinding wheel, workpiece, and fluid, respectively; °C
ρ_G, ρ_W, ρ_F	density of grinding wheel, workpiece, and fluid, respectively; Kg/m^3
τ	friction force; N
ω	angular speed of grinding wheel; rpm
Ω_G, Ω_W	domains of grinding wheel and workpiece

INTRODUCTION

During grinding, a number of physical phenomena occur: cutting, sliding, material removal, heat generation, deformation, fluid flow, etc. This complicated thermomechanical process has attracted intensive attention and research effort over the past decades. The main concern of this machining process is the detrimental effects that high temperatures bring to the workpiece and tool. Coolant is then introduced to remove much of the heat generated between the grinding wheel and the workpiece due to friction and plastic deformation. To gain insight of the heat transfer among individual components in grinding processes, various methods have been proposed. Snoeys *et al.* [1] and Malkin [2] presented detailed reviews of the research conducted on heat transfer in grinding. More recently, Lavine and Jen [3] presented a study which assumed the heat fluxes into the workpiece, grinding wheel, and fluid were uniformly distributed. Later, Jen and Lavine [4] developed an improved model allowing heat flux variation along the grinding zone. This model has been extended and analyzed by Andrew *et al.* [5].

In the paper, first a form of heat source stemming from friction between the grinding wheel and workpiece is proposed. This source term is similar to the one used by Andrews *et al.* [5]. The mathematical model relating the heat transfer between the grinding wheel, fluid, and the workpiece is presented. The finite-element method is employed to numerically solve the problem. Numerical results depicting the temperature profiles of the objects along the grinding zone of the workpiece are shown.

MATHEMATICAL MODEL

In the present study, a two-dimensional setting as depicted in Figure 1, is assumed. Accordingly, all the components involved in the following have the same thickness of one unit in length.

Mathematical Description

Contact Pressure and Heat Source—During grinding, a force is applied to the grinding wheel, Figure 2. This force generates a reaction force, which in turn generates a frictional force that counterbalances the applied turning torque. It is believed that the frictional force is the major heat source of temperature increases in the grinding wheel, workpiece, and cooling fluid. As opposed to the resultant force shown in Figure 2, the reaction from the workpiece should exist in the form of a contact pressure on the grinding wheel. This contact pressure may be difficult to determine as it involves the cooling fluid and the cutting of the workpiece. It is known that,

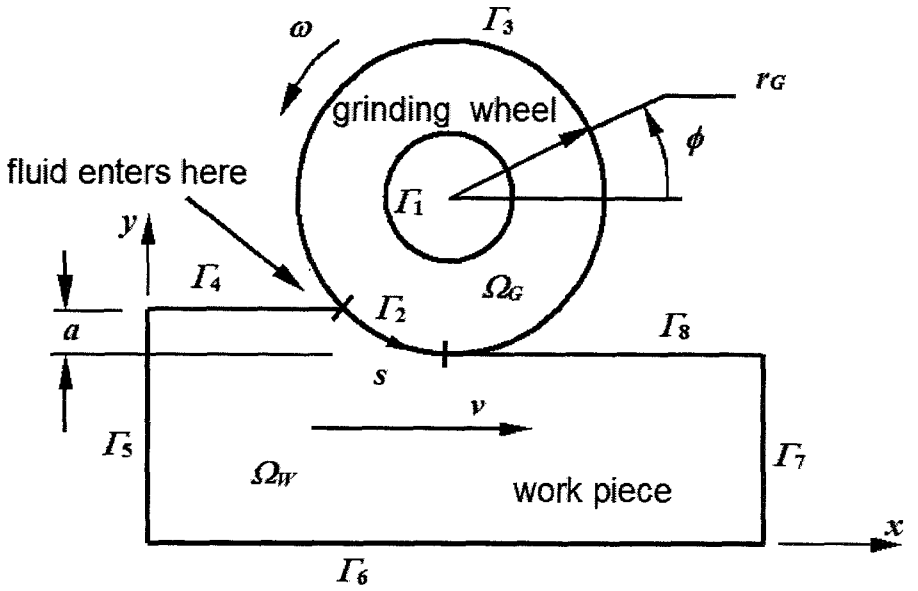

Figure 1. Components in the grinding process.

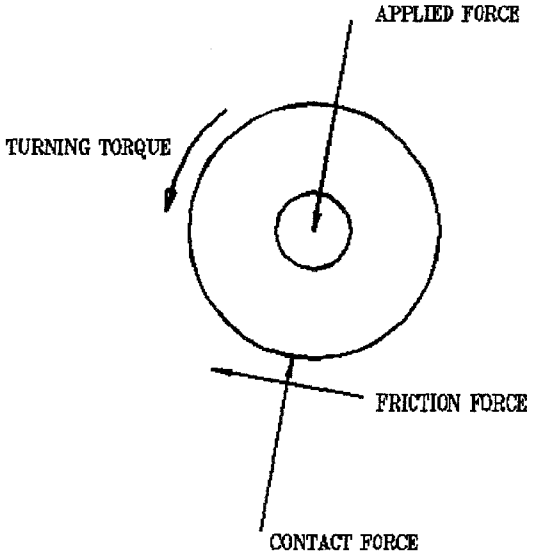

Figure 2. Equilibrium of forces on the grinding wheel.

due to the shape of the grains, the grinding wheel comes into contact with the workpiece only over a small fraction of the grinding area. This allows the coolant to be trapped within the space between the grains. Let this fraction be α, which has a value of $0.05 \sim 0.1$ according to experimental observation. Referring to Figure 3, we assume that the average grain size is d_0, the average contact area of the grain is αd_0, and the contact pressure within the grain contact area is uniform. Thus, each grain exerts a force on the work piece. Recall that the Hertz contact pressure between a cylinder and a plane is elliptical in shape. In the present study, we further assume that these grain forces form an elliptical envelope, as shown in Figure 4. Thus, we have the following form of contact pressure $p(s)$ within the grinding zone $\Gamma_2 = \{s \mid 0 < s < s_l\}$ seen in Figure 1:

$$p(s) = F_0 \sqrt{1 - \left(1 - \frac{2s}{s_l}\right)^2}\, \delta\left(s - \frac{2i-1}{2} d_0\right), \tag{1}$$

where F_0 is the maximum of the elliptical curve, $\delta(\cdot)$ represents the Dirac delta function, and i

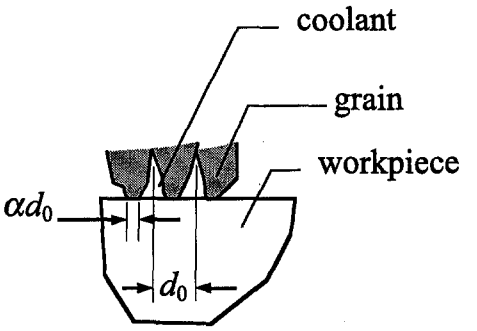

Figure 3. Contact between grain and workpiece.

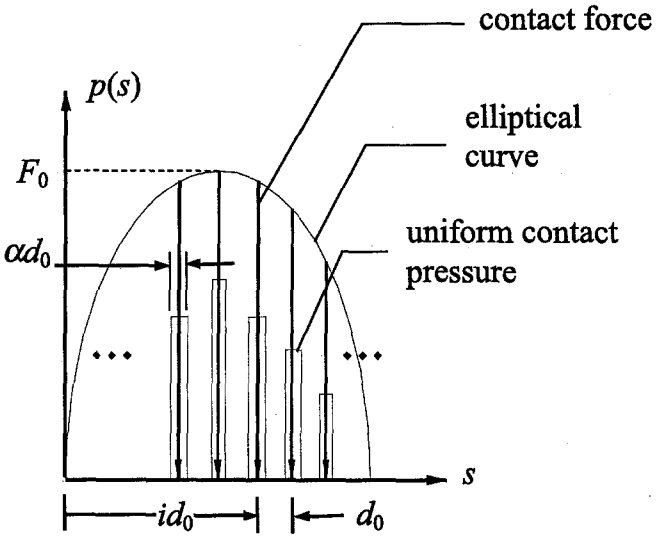

Figure 4. Elliptical distribution of contact forces.

is an index ranging from 1 to n, the number of grains in the grinding zone. To determine F_0, we integrate $p(s)$ over Γ_2 and equate the result to the total applied force F_a.

$$F_0 \sum_{i=1}^{n} \sqrt{1 - \left(1 - \frac{(2i-1)\, d_0}{s_l}\right)^2} = F_a. \tag{2}$$

The friction force seen in Figure 2 is the resultant of the following tangential stress acting on the grinding wheel:

$$\tau = \mu p, \tag{3}$$

where μ is the coefficient of friction and Coulomb's law of friction is employed here. Therefore, the power generated by the friction force, P_i, is

$$P_i = \mu p (r_G \omega - v), \tag{4}$$

where r_G and ω are the radius and angular speed of the grinding wheel, respectively, and v is the velocity of the workpiece. Note that for up-grinding the subtraction sign in equation (4) is replaced by an addition sign, although the difference is minimal for $r_G\omega \gg v$. Jen and Lavine [4] presented a model using uniform and triangular power input, while Kohli [6] showed that a triangular power input is more realistic.

Heat Transfer in Grinding Wheel and Workpiece—The governing equations for the plane heat conduction in the two objects are expressed below.

$$\rho_G c_G \left(\dot{\theta}_G + \omega \theta_{G,\phi}\right) - K_G \Delta \theta_G = 0, \qquad \text{in } \Omega_G, \quad t > 0, \tag{5}$$

and

$$\rho_W c_W \left(\dot{\theta}_W + v\theta_{W,x}\right) - K_W \Delta\theta_W = 0, \qquad \text{in } \Omega_W, \quad t > 0, \tag{6}$$

where the subscripts "G" and "W" indicate that the variable is associated with the grinding wheel or the workpiece, respectively, ρ_G, ρ_W are the densities, c_G, c_W are the specific heat, θ_G, θ_W are the temperatures, a dot over θ_G, or θ_W indicates a partial time derivative, t indicates the time variable, and K_G, K_W are the thermal conductivities. In addition, the comma "," in the above equations denotes the spatial partial derivative, the Δ is the Laplacian operator, and x and ϕ are the horizontal and transverse coordinates as indicated in Figure 1.

The elliptical discrete input power in equation (4) represents the heat source to the grinding system, which does not appear in equations (5) and (6). Instead, it appears in the boundary conditions described below. To divide the heat source between two objects, thermal resistances across the contact area are introduced by Fried [7], Johansson and Klarbring [8], and Johansson [9]. Accordingly, in the case of identical contact objects, the heat source divides evenly for both objects. For lack of experimental evidence, we simply assume that an equal amount of the power enters into the grinding wheel and workpiece, as indicated by the factor "1/2" in the following two equations. Therefore, the boundary conditions along the grinding zone Γ_2 for the two objects are

$$-K_G\theta_{G,n_G} = (1-\alpha)h_F\left(\theta_G - \theta_F\right) + \alpha h_{GW}\left(\theta_G - \theta_W\right) - \frac{1}{2}\mu p(r_G\omega - v), \qquad \text{on } \Gamma_2, \quad t > 0, \tag{7}$$

and,

$$\begin{aligned} -K_W\theta_{W,n_W} = {} & (1-\alpha)h_F\left(\theta_W - \theta_F\right) + \alpha h_{GW}\left(\theta_W - \theta_G\right) \\ & - \frac{1}{2}\mu p(r_G\omega - v) + \rho_W c_W \theta_W g, \qquad \text{on } \Gamma_2, \quad t > 0, \end{aligned} \tag{8}$$

where n_G, n_W are the unit outward normal, h_F is the heat transfer coefficient from the fluid to grinding wheel and workpiece, h_{GW} is the heat transfer coefficient between the grinding wheel and workpiece, θ_F is the temperature in the fluid, and g is the grinding rate (mass of material removed per unit time). The last term on the right-hand side of equation (8) accounts for the energy loss to the chips being removed. We note that only a fraction α of every unit of grinding length is involved in the contact between the grinding grains and the workpiece and the remaining $(1-\alpha)$ is filled with coolant. These fractions can be seen in the above two equations. Pressure dependent thermal conductance to account for the heat transfer between two contact objects has been used by Fried [7], Johansson and Klarbring [8], Johansson [9], and Andrews *et al.* [5]. Here heat transfer coefficients are used between two neighboring objects. These coefficients are difficult to determine, although the average heat transfer coefficients of those derived by Lavine and Jen [3], which are functions of the transverse coordinate, are used in the present study. That is,

$$h_F = \sqrt{\frac{\pi K_F \rho_F c_F r_G \omega}{s_l}}, \tag{9}$$

$$\begin{aligned} h_{GW} = \frac{1}{2}\Bigg[& \frac{1}{s_l}\int_0^{s_l} \sqrt{\frac{\pi K_G \rho_G c_G r_G \omega}{4s}} \frac{2\zeta}{\sqrt{\pi}\left[1 - \exp\left(\zeta^2\right)\operatorname{erfc}(\zeta)\right]}\, ds \\ & + \frac{3}{4}\sqrt{\frac{\pi K_W \rho_W c_W r_G \omega}{\alpha d_0}}\Bigg], \end{aligned} \tag{10}$$

where

$$\zeta = \sqrt{\frac{4K_G s}{\rho_G c_G r_G \omega\, d_0^2}}.$$

Here, K_F, ρ_F, c_F are, respectively, the thermal conductivity, density, and specific heat of the fluid, and $\operatorname{erfc}(\cdot)$ is the error function.

Boundary conditions at the other areas are given below.

$$-K_G\theta_{G,n_G} = 0, \qquad \text{on } \Gamma_1, \qquad t > 0, \tag{11}$$

$$-K_G\theta_{G,n_G} = h\left(\theta_G - \theta_\infty\right), \qquad \text{on } \Gamma_3, \qquad t > 0, \tag{12}$$

$$-K_W\theta_{W,n_W} = 0, \qquad \text{on } \Gamma_5 \cup \Gamma_6 \cup \Gamma_7, \quad t > 0, \tag{13}$$

$$-K_W\theta_{W,n_W} = h\left(\theta_W - \theta_\infty\right), \qquad \text{on } \Gamma_4 \cup \Gamma_8, \qquad t > 0. \tag{14}$$

Here, we assume insulated conditions for the inner wall of the grinding wheel, and the two sides and the bottom surface of the workpiece. The remaining surfaces of the grinding wheel and workpiece have the convective boundary condition allowing heat to dissipate into the ambient air with temperature θ_∞ and heat transfer coefficient h. We also assumed that the initial temperatures of the two objects are equal to the room temperature θ_∞. Thus,

$$\theta_G = \theta_\infty, \qquad \text{in } \Omega_G, \quad \text{as } t = 0, \tag{15}$$

$$\theta_W = \theta_\infty, \qquad \text{in } \Omega_W, \quad \text{as } t = 0. \tag{16}$$

Heat Transfer in Fluid—We now present the governing equation and boundary conditions for the coolant. First, we assume that the coolant is a one-dimensional continuous object whose heat transfer is governed by the following equation in the grinding zone.

$$\rho_F c_F\left(\theta_{F,t} + r_G\omega\theta_{F,s}\right) - K_F\theta_{F,ss} + \frac{(1-\alpha)}{b}\left[h_F\left(\theta_F - \theta_G\right) + h_F\left(\theta_F - \theta_W\right)\right] = 0, \qquad \text{in } \Gamma_2 = \{s \mid 0 < s < s_l\}, \tag{17}$$

where θ_F is the temperature of the fluid and b is the uniform thickness of the fluid. We assume that there is no boiling in the fluid, although its effect is included in a study by Jen and Lavine [10]. In addition, we also assume that the fluid only exists in the grinding zone, although it may spread to other areas in actual operation. The fluid enters the system continuously at the position indicated in Figure 1 and is assumed to be present before grinding starts. Therefore, we have the following boundary and initial conditions.

$$\theta_F = \theta_\infty, \qquad \text{at } s = 0, \tag{18}$$

$$-K_F\theta_{F,s} = h\left(\theta_F - \theta_\infty\right), \qquad \text{at } s = s_l, \tag{19}$$

$$\theta_F = \theta_\infty, \qquad \text{in } \Gamma_2, \quad \text{as } t = 0. \tag{20}$$

Here, we assume that when the fluid exits the grinding zone, the heat dissipates into the ambient air.

Weak Form

Let ϕ_j and φ_j be the one- and two-dimensional weighting functions, respectively. The weak statement of the above initial-boundary-value problem can be formulated as follows.

Grinding Wheel

$$\begin{aligned}
&\int_{\Omega_G} \rho_G c_G\left(\dot{\theta}_G + \omega\theta_{G,\phi}\right)\varphi_j\, d\Omega + \int_{\Omega_G} K_G\theta_{G,i}\varphi_{j,i}\, d\Omega + \int_{\Gamma_3} h_{GW}\theta_G\varphi_j\, d\Gamma \\
&+ \int_{\Gamma_2}\left[(1-\alpha)h_F + \alpha h_{GW}\right]\theta_G\varphi_j\, d\Gamma - \int_{\Gamma_2}(1-\alpha)h_F\theta_F\varphi_j\, d\Gamma - \int_{\Gamma_2}\alpha h_{GW}\theta_W\varphi_j\, d\Gamma \\
&= \int_{\Gamma_3} h_{GW}\theta_\infty\varphi_j\, d\Gamma + \frac{1}{2}\int_{\Gamma_2}\mu p r_G\omega\varphi_j\, d\Gamma.
\end{aligned} \tag{21}$$

Work Piece

$$\int_{\Omega_W} \rho_W c_W \left(\dot{\theta}_W + v\theta_{W,x}\right)\varphi_j \, d\Omega + \int_{\Omega_W} K_W \theta_{W,i}\varphi_{j,i} \, d\Omega + \int_{\Gamma_4 \cup \Gamma_8} h_{GW}\theta_W \varphi_j \, d\Gamma$$
$$+ \int_{\Gamma_2} [(1-\alpha)h_F + \alpha h_{GW} + \rho_W c_W g]\,\theta_W \varphi_j \, d\Gamma - \int_{\Gamma_2} (1-\alpha)h_F \theta_F \varphi_j \, d\Gamma \tag{22}$$
$$- \int_{\Gamma_2} \alpha h_{GW}\theta_G \varphi_j \, d\Gamma = \int_{\Gamma_4 \cup \Gamma_8} h_{GW}\theta_\infty \varphi_j \, d\Gamma + \frac{1}{2}\int_{\Gamma_2} \mu p r_G \omega \varphi_j \, d\Gamma.$$

Fluid

$$\int_{\Gamma_2} \rho_F c_F \left(\dot{\theta}_F + r_G \omega \theta_{F,s}\right)\phi_j \, d\Gamma + \int_{\Gamma_2} K_F \theta_{F,s}\phi_{j,s} \, d\Gamma + \int_{\Gamma_2} \frac{2(1-\alpha)}{b} h_F \theta_F \phi_j \, d\Gamma$$
$$- \int_{\Gamma_2} \frac{1-\alpha}{b} h_F \theta_G \phi_j \, d\Gamma - \int_{\Gamma_2} \frac{1-\alpha}{b} h_F \theta_W \phi_j \, d\Gamma + h\theta_{Fs_l}\phi_{js_l} = h\theta_\infty \phi_{js_l} + \bar{q}_0 \phi_{j0}. \tag{23}$$

In the above and hereafter, the indicial summation convention is implied. However, no summation occurs over the subscript s. Note that $\phi_{js_l} = \phi_j(s_l)$, $\phi_{j0} = \phi_j(0)$, $\theta_{Fs_l} = \theta_F(s_l)$, and $\bar{q}_0$ is the heat flux of the fluid at $s = 0$.

NUMERICAL ALGORITHM

Petrov-Galerkin Approximate Solution

The angular speed of the grinding wheel is so high that the convective effect turns out to be dominant in heat transfer. Therefore, we use the Petrov-Galerkin weighted residual finite-element method to solve the problem numerically. That is, the weighting function and the interpolation functions are different. Let η_k and ψ_k be the one- and two-dimensional linear interpolation functions, then the temperatures can be approximated as follows.

$$\theta_G = \psi_k \Theta_{Gk}, \qquad \theta_W = \psi_k \Theta_{Wk}, \qquad \theta_F = \eta_k \Theta_{Fk}. \tag{24}$$

Choose the weighting functions as

$$\varphi_j = \psi_j + \beta v_l \psi_{j,l}; \qquad \phi_j = \eta_j + \beta r_G \omega \eta_{j,s}, \tag{25}$$

where β is a parameter which will be chosen later. This weighting functions are applied to all the terms in the above except the time-derivative terms resulting in an algorithm similar to that reported by L–hner *et al.* [11]. Substitution of the above two equations into equations (21)–(23) yields the following finite-element equations.

Grinding Wheel

$$\int_{\Omega_G} \rho_G c_G \psi_j \psi_k \, d\Omega \dot{\Theta}_{Gk} + \int_{\Omega_G} \rho_G c_G \omega(\psi_j + \beta v_l \psi_{j,l})\psi_{k,\phi} \, d\Omega \Theta_{Gk} + \int_{\Omega_G} K_G \psi_{j,i}\psi_{k,i} \, d\Omega \Theta_{Gk}$$
$$+ \int_{\Gamma_3} h_{GW}(\psi_j + \beta v_l \psi_{j,l})\psi_k \, d\Gamma \Theta_{Gk} + \int_{\Gamma_2} [(1-\alpha)h_F + \alpha h_{GW}](\psi_j + \beta v_l \psi_{j,l})\psi_k \, d\Gamma \Theta_{Gk}$$
$$- \int_{\Gamma_2} (1-\alpha)h_F(\psi_j + \beta v_l \psi_{j,l})\psi_k \, d\Gamma \Theta_{Fk} - \int_{\Gamma_2} \alpha h_{GW}(\psi_j + \beta v_l \psi_{j,l})\psi_k \, d\Gamma \Theta_{Wk} \tag{26}$$
$$= \int_{\Gamma_3} h_{GW}\theta_\infty(\psi_j + \beta v_l \psi_{j,l}) \, d\Gamma + \frac{1}{2}\int_{\Gamma_2} \mu p r_G \omega(\psi_j + \beta v_l \psi_{j,l}) \, d\Gamma.$$

Work Piece

$$\begin{aligned}
&\int_{\Omega_W} \rho_W c_W \psi_j \psi_k \, d\Omega \dot{\Theta}_{Wk} + \int_{\Omega_W} \rho_W c_W v(\psi_j + \beta v \psi_{j,x}) \psi_{k,x} \, d\Omega \Theta_{Wk} \\
&+ \int_{\Omega_W} K_W \psi_{j,i} \psi_{k,i} \, d\Omega \Theta_{Wk} + \int_{\Gamma_4 \cup \Gamma_8} h_{GW} (\psi_j + \beta v \psi_{j,x}) \psi_k \, d\Gamma \Theta_{Wk} \\
&+ \int_{\Gamma_2} [(1-\alpha) h_F + \alpha h_{GW} + \rho_W c_W g] (\psi_j + \beta v \psi_{j,x}) \psi_k \, d\Gamma \Theta_{Wk} \\
&- \int_{\Gamma_2} (1-\alpha) h_F (\psi_j + \beta v \psi_{j,x}) \psi_k \, d\Gamma \Theta_{Fk} - \int_{\Gamma_2} \alpha h_{GW} (\psi_j + \beta v \psi_{j,x}) \psi_k \, d\Gamma \Theta_{Gk} \\
&= \int_{\Gamma_4 \cup \Gamma_8} h_{GW} \theta_\infty (\psi_j + \beta v \psi_{j,x}) \, d\Gamma + \frac{1}{2} \int_{\Gamma_2} \mu p r_G \omega (\psi_j + \beta v \psi_{j,x}) \, d\Gamma .
\end{aligned} \tag{27}$$

Fluid

$$\begin{aligned}
&\int_{\Gamma_2} \rho_F c_F \eta_j \eta_k \, d\Gamma \dot{\Theta}_{Fk} + \int_{\Gamma_2} \rho_F c_F r_G \omega (\eta_j + \beta r_G \omega \eta_{j,s}) \eta_{k,s} \, d\Gamma \Theta_{Fk} + \int_{\Gamma_2} K_F \eta_{j,s} \eta_{k,s} \, d\Gamma \Theta_{Fk} \\
&+ \int_{\Gamma_2} \frac{2(1-\alpha)}{b} h_F (\eta_j + \beta r_G \omega \eta_{j,s}) \eta_k \, d\Gamma \Theta_{Fk} - \int_{\Gamma_2} \frac{1-\alpha}{b} h_F (\eta_j + \beta r_G \omega \eta_{j,s}) \bar{\psi}_k \, d\Gamma \Theta_{Gk} \\
&- \int_{\Gamma_2} \frac{1-\alpha}{b} h_F (\eta_j + \beta r_G \omega \eta_{j,s}) \bar{\psi}_k \, d\Gamma \Theta_{Wk} + h \left[(\eta_j + \beta r_G \omega \eta_{j,s}) \eta_k \right]_{s_l} \Theta_{Fk} \\
&= h \theta_\infty \left[(\eta_j + \beta r_G \omega \eta_{j,s}) \eta_k \right]_{s_l} + \bar{q}_0 \left(\eta_j + \beta r_G \omega \eta_{j,s} \right)_0 .
\end{aligned} \tag{28}$$

Note that the second-order derivatives of η_k and ψ_k vanish, since they are linear functions of the natural coordinates. The subscripts "s_l" and "0" indicate that the associated quantities are evaluated at $s = s_l$ and s=0, respectively, and $\bar{\psi}_k$ is ψ_k evaluated at the element edge on boundary Γ_2. Moreover, the workpiece only moves in the x-direction with velocity v. Although the convective effect due to this velocity is much smaller that that of the grinding wheel, it is retained in the equation for integrity.

Time Integration

The time derivative terms in the above three equations are discretized using the following implicit integration scheme.

$$\frac{\Delta \Theta_{Gk}}{\Delta t} = \lambda \dot{\Theta}_{Gk}^{n+1} + (1-\lambda) \dot{\Theta}_{Gk}^{n}, \tag{29}$$

where the superscript n designates the time step, Δt is the time step size, and $0 \leq \lambda \leq 1$. Thus,

$$\dot{\Theta}_{Gk}^{n+1} = \frac{1}{\lambda} \left[\frac{1}{\Delta t} \Delta \Theta_{Gk} - (1-\lambda) \dot{\Theta}_{Gk}^{n} \right], \tag{30}$$

and at the time step $n+1$, equation [26] becomes

$$\begin{aligned}
&\left(\frac{1}{\Delta t} A_{jk}^G + \lambda \left(B_{jk}^G + C_{jk} + D_{jk} \right) \right) \Delta \Theta_{Gk} - \lambda C_{jk} \Delta \Theta_{Fk} - \lambda D_{jk} \Delta \Theta_{Wk} \\
&= \lambda R_k^{n+1} + (1-\lambda) A_{jk}^G \dot{\Theta}_{Gk}^n - \lambda \left(B_{jk}^G + C_{jk} + D_{jk} \right) \Theta_{Gk}^n + \lambda C_{jk} \Theta_{Fk}^n + \lambda D_{jk} \Theta_{Wk}^n ,
\end{aligned} \tag{31}$$

where

$$
\begin{aligned}
A_{jk}^{G} &= \int_{\Omega_G} \rho_G c_G \psi_j \psi_k \, d\Omega, \\
B_{jk}^{G} &= \int_{\Omega_G} \rho_G c_G \omega (\psi_j + \beta v_l \psi_{j,l}) \psi_{k,\phi} \, d\Omega + \int_{\Omega_G} K_G \psi_{j,i} \psi_{k,i} \, d\Omega \\
&\quad + \int_{\Gamma_3} h_{GW} (\psi_j + \beta v_l \psi_{j,l}) \psi_k \, d\Gamma, \\
C_{jk} &= \int_{\Gamma_2} (1-\alpha) h_F (\psi_j + \beta v_l \psi_{j,l}) \psi_k \, d\Gamma, \\
D_{jk} &= \int_{\Gamma_2} \alpha h_{GW} (\psi_j + \beta v_l \psi_{j,l}) \psi_k \, d\Gamma, \\
R_k &= \int_{\Gamma_3} h_{GW} \theta_\infty (\psi_j + \beta v_l \psi_{j,l}) \, d\Gamma + \frac{1}{2} \int_{\Gamma_2} \mu p r_G \omega (\psi_j + \beta v_l \psi_{j,l}) \, d\Gamma.
\end{aligned}
\tag{32}
$$

Similar equations for the workpiece and fluid can be obtained from equations (27) and (28). Thus, we have a system of algebraic equations for solving the evolving temperatures in the components.

NUMERICAL SIMULATION AND DISCUSSION

The material constants and parameters used in the simulation are given in Tables 1 and 2 which are mainly from [4]. Let $\beta = \Delta t/2$ according to [11], and for numerical stability, $\lambda = 0.5$ is used. The thickness of the fluid is chosen to be half of the grit size, i.e., $b = d_0/2$. The grit size is $d_0 = 0.5\,\text{mm}$ which is equivalent to the commercial size of No. 50. The current model is two-dimensional, so the thickness of the grinding wheel is assumed to be the same as that of the workpiece. Consequently, the applied force F_a of 10 kN is used in the following simulations. Furthermore, the coefficients of friction used are $\mu = 0.3$ and 0.4. Also, the size of the time step used is $\Delta t = 0.1\,\text{s}$, and the total time step used is 1,500 for a duration of 2.5 minutes.

Table 1. Material constants of components in a grinding process.

	Grinding Wheel Al_2O_3	Workpiece steel	Fluid water
ρ, kg/m^3	4000	7854	1000
c, J/kg-K	770	434	4180
K, W/m-K	46	60.5	0.68

Table 2. System parameters used in numerical simulation.

a, mm	α	ω, rpm	Δt, sec	b, mm	θ_∞, °C	v, mm/sec	r_G, m	d_0, mm
0.5	0.05	2865	10^{-2}	0.25	20	1.0	0.1	0.5

A finite-element model containing 489 elements and 546 nodes for the grinding wheel and 794 elements and 845 nodes for the workpiece is created. There are eight fluid elements along the grinding zone. Note that none of the elements share common nodes. Figure 5 shows the finite-element mesh used in the numerical simulation. The evolving temperature-increase ($\Delta\theta = \theta - \theta_\infty$) of the workpiece along the grinding zone is depicted in Figure 6 by the solid lines when the applied force $F_a = 10\,\text{kN}$, $\mu = 0.3$, and Hertzian contact pressure equation (1) are used. It is seen that the temperature reaches steady-state condition when $t = 150\,\text{sec}$. Note that the temperature-increase at the point where the coolant is introduced ($s = 0\,\text{mm}$) is higher than at the point where the coolant exits ($s = 10\,\text{mm}$) by about 7°C at $t = 150\,\text{s}$. The stabilized temperature-increase

contour of the system near the grinding zone is shown in Figure 7. It is seen that most the area in the workpiece has a temperature-increase of less than 5°C. Note that the workpiece travels to the right at a slow speed. The temperature-increase for the grinding wheel is 48°C at $t = 150$ s. It is rather uniform, although that it is 1°C higher near the center of the grinding zone. The temperature-increase for the coolant is rather low and is depicted in Figure 6 by dashed lines for only three time steps. This is due to the fact that the coolant stays in the grinding zone for a very short period of time.

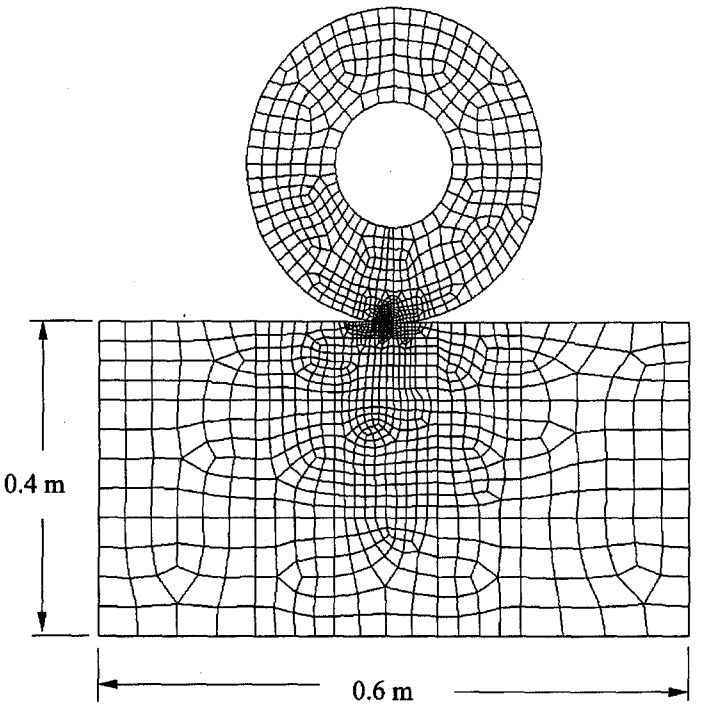

Figure 5. Finite-element mesh used in simulation calculation.

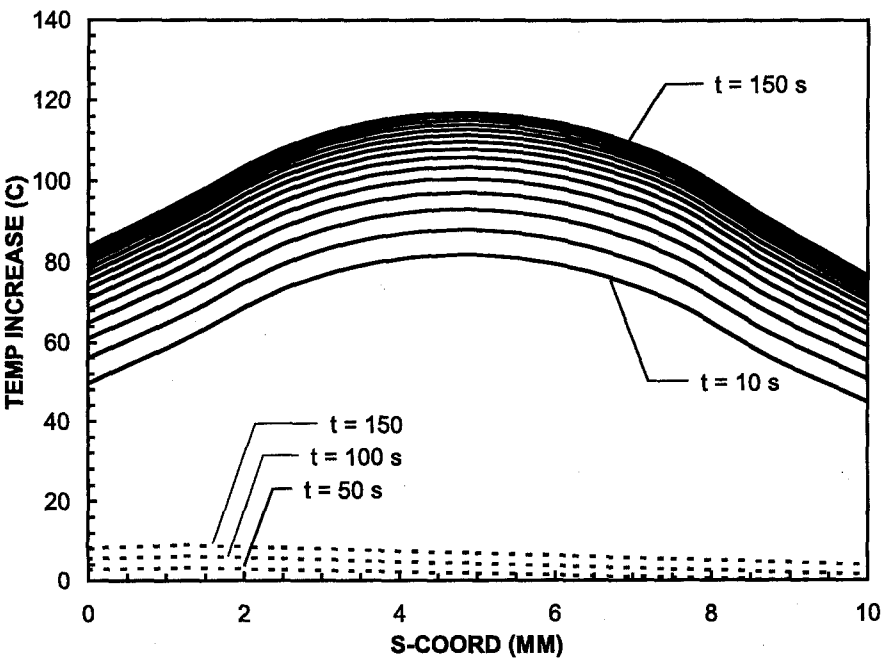

Figure 6. Temperature-increase of the coolant (dashed lines) and the workpiece (solid lines) along the grinding zone.

A triangular pressure profile has been used by Jen and Lavine [4] and Kohli [6]. For comparison purpose, the following triangular pressure profile is also used in the simulation.

$$p(s) = 2F_0 \frac{s}{s_l} - 4F_0 \left(\frac{s}{s_l} - \frac{1}{2}\right) U\left(\frac{s}{s_l} - \frac{1}{2}\right) \delta\left(s - \frac{2i-1}{2} d_0\right), \qquad 0 < s < s_l, \tag{33}$$

where $U(\cdot)$ is the Heaviside unit step function. The constant F_0 can be evaluated in the same fashion as in equation (2). The stabilized ($t = 150\,\mathrm{s}$) temperature-increase for the workpiece along the grinding zone is shown in Figure 8, where two coefficients of friction ($\mu = 0.3, 0.4$) are used. Since the maximum pressure for the triangular profile is greater than that of the Hertzian profile, its maximum temperature-increase at the middle of the grinding zone is seen to be higher than that of the Hertzian profile. Figure 9 shows the evolution of the maximum temperature-increases using different contact pressure profiles and coefficients of friction.

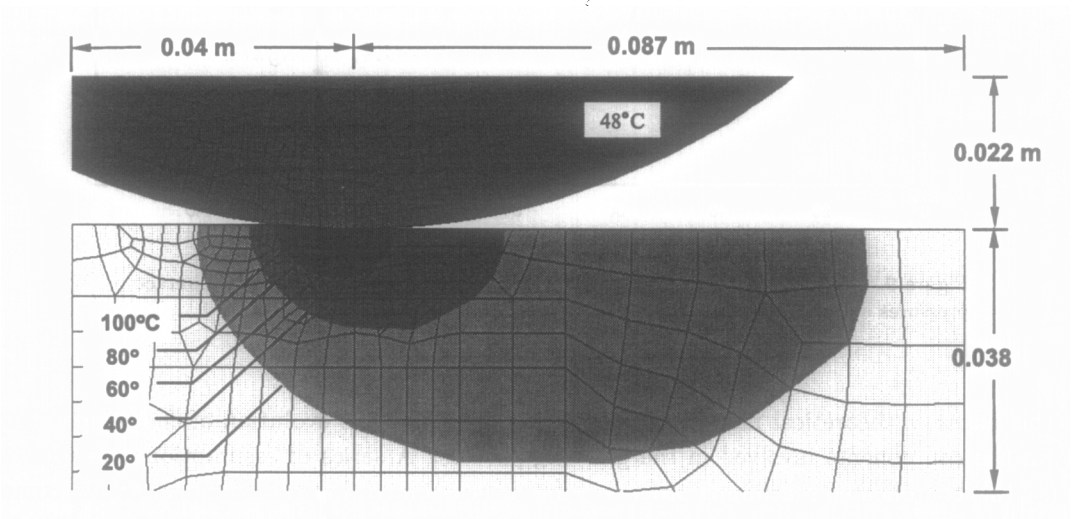

Figure 7. Stabilized temperature-increase profile.

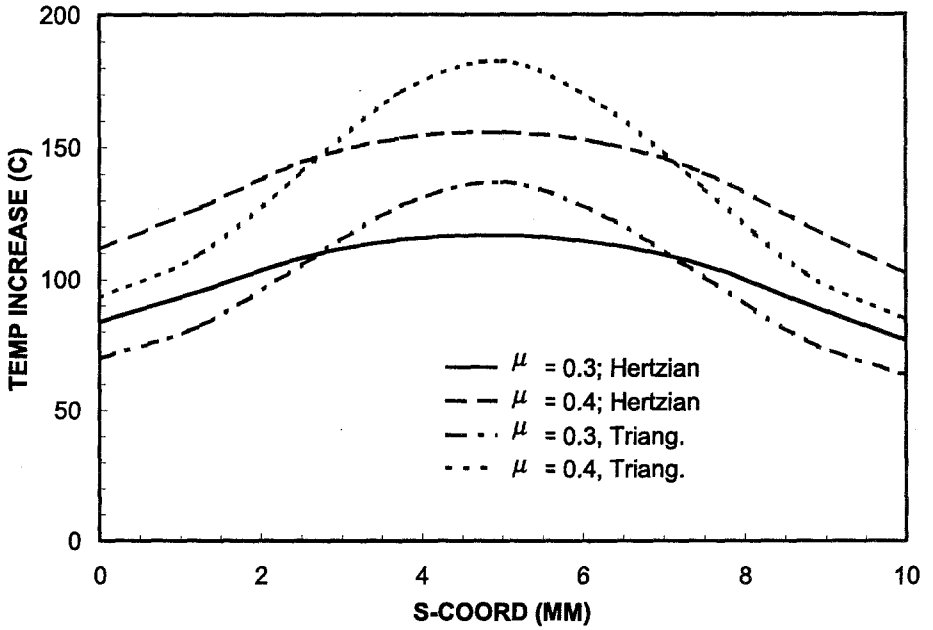

Figure 8. Comparison of temperature-increases in the workpiece along the grinding zone using various contact pressures and coefficients of friction.

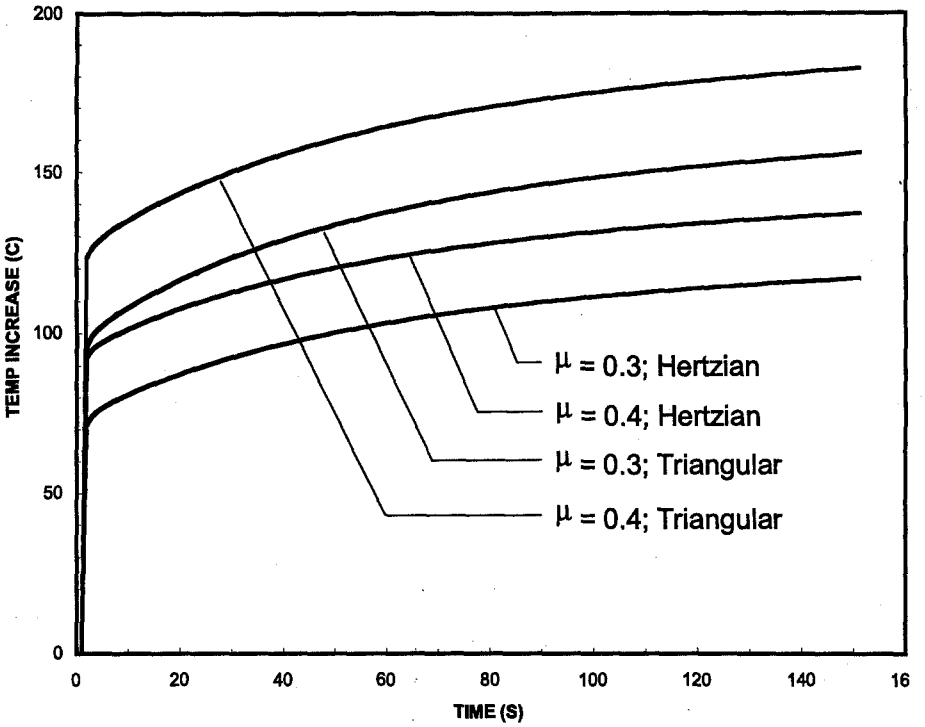

Figure 9. Evolution of the maximum temperature-increases using different contact pressures and coefficients of friction.

CONCLUSIONS

In this paper, a theoretical model is presented to determine the evolution of the temperature fields in the components involved in the grinding process. A series of assumptions are used to simplify this complicated machining process. First, it is assumed that the only heat source comes from the friction between the grinding wheel and workpiece modeled as two-dimensional objects. A Hertzian form of contact pressure is assumed for calculating the frictional force. The coolant, modeled as a one-dimensional object, is introduced to dissipate the heat along the grinding zone. In addition, heat also flows to the ambient environment through convection. The heat transfer between the neighboring objects is modeled by convection. Heat transfer coefficients established by other researchers are used in this regard. The finite-element method is employed to discretize the system of differential equations in spatial coordinates while an implicit integration scheme is applied to the time domain. Numerical results presented include the temperature-rises in the grinding wheel and workpiece using Hertzian contact pressure and triangular contact pressure. Different values of coefficient of friction are also used in the calculation to show its effects on the temperature-rise.

REFERENCES

1. R. Snoeys, M. Maris and J. Peters, Thermally induced damage in grinding, *CIRP Annals* **27** (2), 571–581, (1978).
2. S. Malkins, Grinding of metals: Theory and application, *J. Applied Metalworking* **3** (2), 95–109, (1984).
3. A.S. Lavine and T.-C. Jen, Coupled heat transfer to workpiece, wheel, and fluid in grinding, and the occurrence of workpiece burn, *Int. J. of Heat Mass Transfer* **34** (4/5), 983–992, (1991).
4. T.-C. Jen and A.S. Lavine, A variable heat flux model of heat transfer in grinding: Model development, *ASME J. of Heat Transfer* **117**, 473–478, (1995).
5. K.T. Andrews, M. Shillor and S. Wright, A model for heat transfer in grinding, *Nonlinear Analysis* **35**, 233–246, (1999).
6. S. Kohli, Energy partition for grinding with aluminum oxide and cubic boron nitride abrasive wheels, Department of Mechanical Engineering, University of Massachusetts, (1993).
7. E. Fried, Thermal conduction contribution to heat transfer at contacts, In *Thermal Conductivity, Volume 2*, (Edited by R.P. Tye), Academic Press, London, (1969).

8. L. Johansson and A. Klarbring, Thermoelastic frictional contact problems: Modelling, finite element approximation and numerical realization, *Computer Meth. Applied Mech. and Engineering* **105**, 181–210, (1993).
9. L. Johansson, Model and numerical algorithm for sliding contact between two elastic half-planes with frictional heat generation and wear, *Int. J. on the Sci. and Tech. of Friction, Lubrication, and Wear* **160** (1), 77–94, (1993).
10. T.-C. Jen and A.S. Lavine, A variable heat flux model of heat transfer in grinding with boiling, *ASME J. of Heat Transfer* **118**, 463–470, (1996).
11. R. L–hner, K. Morgan and O.C. Zienkiewicz, The solution of non-linear hyperbolic equation systems by the finite element method, *Int. J. Num. Meth. Eng.* **4**, 1043–1063, (1984).
12. I. Christie, D.F. Griffiths, A.R. Mitchell and O.C. Zienkiewicz, Finite element methods for second order differential equations with significant first derivatives, *Int. J. Num. Meth. Eng.* **10**, 1389–1396, (1976).
13. T.J.R. Hughes and A. Brooks, A multi-dimensional upwind scheme with no cross wind diffusion, In *Finite Elements for Convection Dominated Flows*, AMD 34, ASME, (Edited by T.J.R. Hughes), (1979).
14. D.W. Kelly, S. Nakazawa and O.C. Ziekiewicz, A note on anisotropic balancing dissipation in the finite element method approximation to convective diffusion problems, *Int. J. Num. Meth. Eng.* **15**, 1705–1711, (1980).